Naval Research Laboratory

Washington, DC 20375-5320

NRL/MR/6171--20-10,032

3D Nanostructured Plasmonic Photocatalysis

Paul A. DeSario
Debra R. Rolison

Surface Chemistry Branch
Chemistry Division

January 28, 2021

REPORT DOCUMENTATION PAGE

Form Approved
OMB No. 0704-0188

1. REPORT DATE *(DD-MM-YYYY)*	**2. REPORT TYPE**	**3. DATES COVERED** *(From - To)*
28-01-2020	NRL Memorandum Report	1 Oct 15 – 30 Sept 19

4. TITLE AND SUBTITLE

3D Nanostructured Plasmonic Photocatalysis

5a. CONTRACT NUMBER

5b. GRANT NUMBER

5c. PROGRAM ELEMENT NUMBER
61153N

6. AUTHOR(S)

Paul A. DeSario and Debra R. Rolison

5d. PROJECT NUMBER

5e. TASK NUMBER

5f. WORK UNIT NUMBER
1C22

7. PERFORMING ORGANIZATION NAME(S) AND ADDRESS(ES)

Naval Research Laboratory
4555 Overlook Avenue, SW
Washington, DC 20375-5320

8. PERFORMING ORGANIZATION REPORT NUMBER

NRL/MR/6171--20-10,032

9. SPONSORING / MONITORING AGENCY NAME(S) AND ADDRESS(ES)

10. SPONSOR / MONITOR'S ACRONYM(S)

11. SPONSOR / MONITOR'S REPORT NUMBER(S)

12. DISTRIBUTION / AVAILABILITY STATEMENT

DISTRIBUTION STATEMENT A: Approved for public release distribution is unlimited.

13. SUPPLEMENTARY NOTES

14. ABSTRACT

15. SUBJECT TERMS

16. SECURITY CLASSIFICATION OF:			**17. LIMITATION OF ABSTRACT**	**18. NUMBER OF PAGES**	**19a. NAME OF RESPONSIBLE PERSON**
a. REPORT	**b. ABSTRACT**	**c. THIS PAGE**			Paul DeSario
Unclassified Unlimited	Unclassified Unlimited	Unclassified Unlimited	Unclassified Unlimited	24	**19b. TELEPHONE NUMBER** *(include area code)* (202) 767-0417

This page intentionally left blank.

CONTENTS

This page intentionally left blank.

3D NANOSTRUCTURED PLASMONIC PHOTOCATALYSIS

1. INTRODUCTION

We describe a multi-disciplinary, fundamental study of the design of a class of catalytic materials that utilize sunlight to: 1) enable delivery of fuels (hydrogen) and fuel feedstocks (methane, methanol) to the Navy using water and carbon dioxide as starting materials; or 2) efficiently degrade toxic contaminants, including organophosphorus compounds. Solar-driven photocatalytic water splitting and reduction of carbon dioxide are two of the highest payoff pathways to carbon-neutral fuels. Additionally, adding sunlight-driven photocatalytic activity to adsorptive and degradative materials can enhance decontamination capacity.

Currently, there are no stand-alone semiconductor photocatalysts that simultaneously combine efficient light harvesting, long exciton lifetimes, and catalytic selectivity. We describe an approach to photocatalyst design wherein the individual functions of the photocatalyst are integrated within a nanocomposite material. Within these composites, light-harvesting "antennae" are physically separated from, yet electronically wired to, catalytically active sites. Our composite materials platform comprise a high-surface-area titania (TiO_2) aerogel with incorporated gold nanoparticles (Au–TiO_2) that feature (a) Au surface plasmon resonance (SPR)-sensitized photocatalytic activity that spans a broad portion of the visible spectrum and (b) enhanced electron–hole lifetimes courtesy of the 3-D interconnected oxide network. Crucially, the Au guest is entrained within the 3-D network of covalently bonded oxide nanoparticles: configuring Au||TiO_2 interfaces in 3-D doubles the rate of visible-light driven photocatalytic water splitting over those produced when Au of the same size and shape is deposited on pre-formed TiO_2 aerogels. The objective of this fundamental research program is to synthesize the materials and execute the experiments that enable detailed analysis of the plasmonic sensitization mechanism, identify nanoscale design parameters that control plasmonic-sensitization efficiency, and understand the effect of the networked oxide on charge transport and excited state lifetimes. Elucidating these fundamental mechanisms, physical phenomena, and materials design rules is the crucial first step in exploiting these porous nanostructured materials for solar fuels photocatalysis and sunlight-assisted degradation.

2. BACKGROUND

The primary variables limiting the performance of photocatalytic semiconductors include: 1) inefficient absorption of incident light, especially in the visible, 2) limited lifetimes of photo-generated carriers, and 3) poor selectivity for the reactions of interest. Titanium dioxide (TiO_2) is one of the most highly investigated semiconductors for photocatalytic applications because it is chemically stable and inexpensive. For energy applications, TiO_2 is desirable because its band energies provide sufficient thermodynamic potential to drive total water splitting [1] and its conduction band (CB) electrons have sufficient thermodynamic potential for CO_2 reduction. The CB holes of TiO_2 have sufficient energy to produce highly oxidizing radical species, thus making TiO_2 an attractive catalyst for degradation and remediation applications.

As a tradeoff of its large bandgap (3.2 eV for anatase), TiO_2 requires ultraviolet light (UV) for excitation, which greatly limits its practical applications. One chemically robust means of sensitizing TiO_2 to visible light and expanding its applicability for solar-driven technologies is coupling with plasmonic sensitizers that have a SPR in the visible. As a plasmonic sensitizer, gold (Au) offers advantages over silver (Ag):

Manuscript approved January 25, 2021.

it's more stable against oxidation and has broader overlap with the most intense region of the solar spectrum [2,3,4,5,6]. Copper (Cu) also has a plasmon resonance in the visible, however, its utilization has been limited by its propensity to oxidize at the expense of its plasmon resonance.

Aerogels are appealing materials for catalytic applications and as supports for plasmonic nanoparticles because of their inherent physical features. They provide high specific surface areas (100–1000 m^2 g^{-1}), low density, ample free volume, and a continuous mesoporous network. The high surface area of aerogels multiplies reactive sites while the continuous mesoporous network enables rapid flux of reactants to and products from those sites [7,8,9,10,11,12,13]. Additionally, materials with high surface areas absorb and internally scatter light very effectively, thus improving photon harvesting [14,15,16,17]. The intimate interfacial contact between TiO_2 aerogels and incorporated Au nanoparticles not only stabilizes the Au nanoparticles against aggregation, even at high-temperature, but also provides an abundant interfacial area for hot carrier injection or resonant energy transfer (Scheme 1) [7,18].

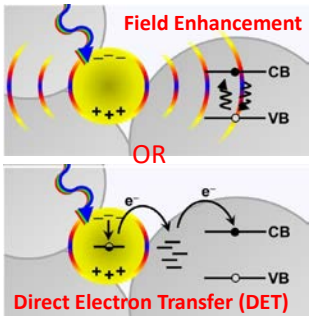

Scheme 1

The proven ability of incorporated Au nanoparticles to sensitize photoelectrochemical water-splitting reactions at Au–TiO_2 aerogels at visible wavelengths extending to >700 nm [18], coupled with the design flexibility available to Au–TiO_2 in terms of surface area, porosity, and size of the oxide support and weight fractions of incorporated Au nanoparticles [7,18] make it a powerful candidate with which to start unraveling the critical parameters for designing and improving visible-light-active photocatalysts on the nanoscale.

3. TECHNICAL APPROACH

We exploit the design flexibility of composite aerogels [7,14,18,19,20,21] by varying the size, weight fraction, and composition of guest nanoparticles, as well as the fundamental dimensions of the oxide network, to create materials that enable us to: (1) elucidate the multiple visible-light SPR sensitization mechanisms of TiO_2 by Au that drive photocatalysis; (2) use insights derived from (1) to modify the nanoscale design of Au–TiO_2; (3) use 3-D networked nanoscale oxides to enhance electron–hole lifetimes; and (4) incorporate the appropriate co-catalysts that efficiently catalyze oxidation (ex. H_2O oxidation, oxidation of organophosphates) or reduction reactions (ex. CO_2 reduction, water reduction), separately or in tandem (Figure 1). Photocatalytic water splitting, as well as standard photocatalytic diagnostic reactions are characterized in terms of quantum efficiency and product distributions. Effects of Au size, Au||TiO_2 interfacial structure, and TiO_2 aerogel network properties are systematically and independently varied. The synthetic strategy demonstrated with Au–TiO_2 was adapted to Cu nanoparticles as a non-precious alternative to Au. Additional co-catalysts for reduction (Pt) or oxidation (IrO_2) are synthetically wired to plasmonic sensitizers to improve selectivity for reactions of interest.

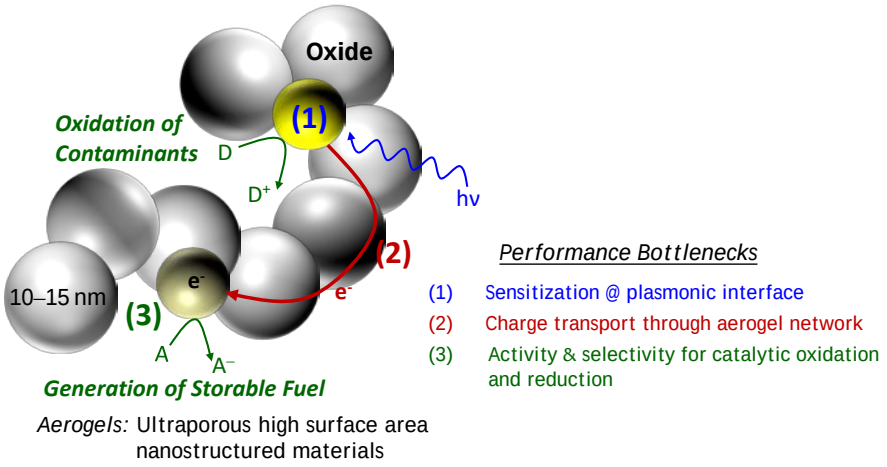

Fig. 1 — Schematic diagram of composite TiO_2 aerogels featuring (1) plasmonic nanoparticles supported on or within the oxide, (2) a covalently bonded oxide network with high surface-area and mesoporous voids that physically separates electrons and holes, and (3) a co-catalyst with selective activity for the reaction of interest

We utilize transient spectroscopy spanning multiple timescales (ps—ms) to determine electron-hole pair lifetimes and characterize charge-recombination dynamics as a function of networked oxide properties. Transient spectroscopy is coordinated with first principles calculations of the photocatalyst electronic structure and electrodynamics to understand the fate of photogenerated carriers within the composite material. Modeling of both the plasmonic response and electron transport rates in the catalysts as a function of 3D nanoscale structure will enable us to connect fundamental physics of electron-hole pair generation and transport to photocatalytic performance (i.e., rate and efficiency of photocatalytic generation of fuels).

4. TECHNICAL INSIGHTS AND ACHIVEMENTS

4.1 Carrier Dynamics in the Oxide Network

4.1.1 Correlating Changes in Electron Lifetime and Mobility to Photocatalytic Activity

We utilize dynamic photoelectrochemical methods and direct measurement of photocatalytic hydrogen (H_2) generation to quantify the advantages of networked, ultraporous nanoarchitectures for photocatalysis (Figure 2). Specifically, dynamic techniques are used to demonstrate the effects of modifying the nanoscale dimensions of the supporting TiO_2 aerogel photocatalyst network on both electron transport and trapping [22]. The relationship between electron mobility, trapping, and photocatalytic activity in networked nanoscale photocatalysts had long been speculated, but never previously quantified. Using intensity modulated photovoltage spectroscopy (IMVS) and intensity-modulated photocurrent spectroscopy (IMPS) we obtain the lifetime and mobility of CB and/or trapped electrons for a series of TiO_2 aerogels in which the density of the oxide network is changed. We also acquired ultrafast (sub-nanosecond) electron dynamics on our networked aerogel materials using transient infrared (IR) absorption.

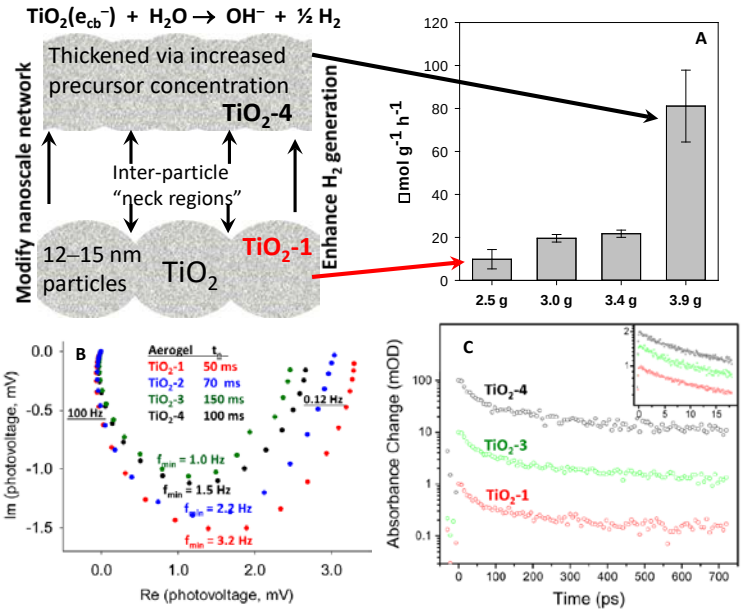

Fig. 2 — Schematic diagram of composite thickened particle—particle junctions in TiO_2; (A) mass-normalized rates of photocatalytic hydrogen generation under broadband illumination over a series of TiO_2 aerogels synthesized with increasing oxide precursor in sol–gel synthesis (TiO_2-1, TiO_2-2, TiO_2-3, and TiO_2-4); (B) complex plane plots of intensity-modulated photovoltage spectroscopy and photoelectrochemical electron lifetimes recorded for TiO_2 aerogels prepared with differing network densities; (4) normalized transient IR decay curves after excitation at 267 nm with probe at 4500 μm and inset showing early time-scale dynamics for TiO_2 aerogels prepared with differing network densities. Adapted from reference 22.

The changes in electron lifetime/mobility have varying impact on photocatalytic reactions depending upon the critical mechanistic steps in the reaction. The lifetimes of photogenerated electrons increase with increased network density indicating an increased site density for electron traps, a trend that correlates with improved activity for photocatalytic hydrogen generation. In contrast, photocatalytic dichloroatetate (DCA) degradation, which is driven by direct hole transfer rather than electron transfer, depends only weakly on electron dynamics [22]. Only electron dynamics captured under photocatalytically relevant conditions, and not those captures on ultrafast timescales (sub-ns) predict photoelectrochemical activity. Correlating hole-mediated and electron-mediated photocatalytic activity with direct measurement of electron dynamics under photocatalytically relevant conditions and time scales is a powerful approach to determine how structural modifications impact relevant physicochemical phenomena underlying photocatalytic performance.

4.1.2 First Principles Calculations of Interfacial Trap States in TiO_2 Aerogels

As characterized by dynamic photoelectrochemical methods (IMVS and IMPS), the catalytic performance of porous, nanocrystalline anatase is strongly affected by the presence of electronic trap states, which are likely incorporated at particle—particle junctions. Trap states delay carrier recombination and act as active sites for catalysis, thus, trap site density is highly correlated to photocatalytic activity. Relative to point defects such as oxygen-vacancies or interstitial atoms, trap states associated with surfaces and interfaces are poorly understood. The energetic and spatial distributions of interfacial trap states were previously not known.

We calculate the electronic structure of interfacially connected anatase nanoparticles using density functional theory (DFT) to search for molecular orbitals at particle-particle junctions and to identify their energies within the bandgap [23]. Two common orientations of anatase particles are compared: one attached by (001) facets and one attached by (101) facets (Figure 3). Our initial approach to computing

the electronic structure of interfacial systems utilized the semi-empirical neglect of differential diatomic overlap (NDDO) approximation, which was selected based on previous studies reported in the literature. However, we have performed extensive validation studies and found that it poorly reproduced measured band gaps and, more critically, trap state depths in nanocrystalline anatase.

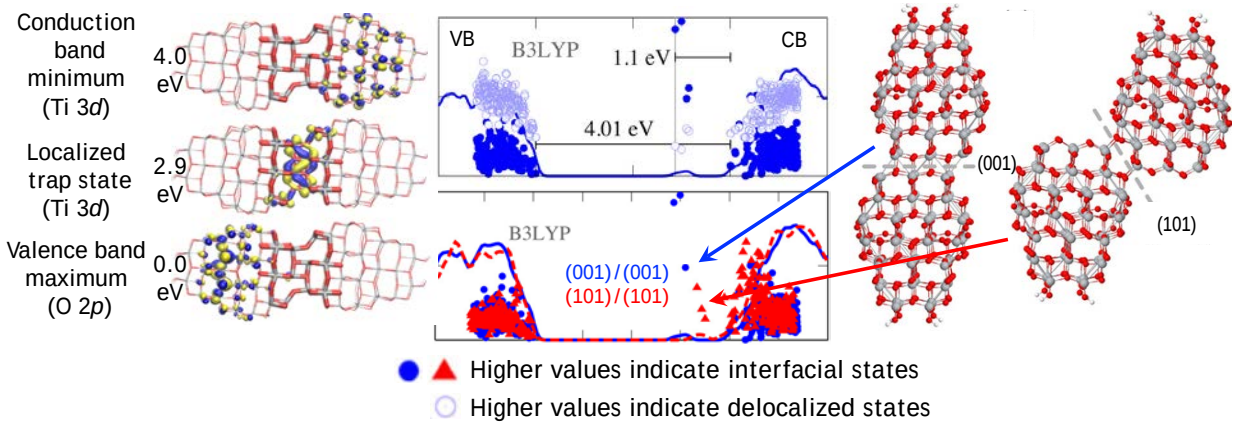

Fig. 3 — LEFT PANEL: examples of three frontier orbitals from the B3LYP//PBE calculation of anatase particles attached on their (001) facets. CENTER PANEL: (top) density of state curves for two particles attached at (001) facets including interfacial states (filled markers) and de-localized states (open markers) from the highest 200 occupied and lowest 200 occupied canonical orbitals; (bottom) electronic densities of states from the highest occupied and lowest 200 unoccupied orbitals for the systems of particles attached on (001) facets (blue) and (101) facets (red). RIGHT PANEL: $(TiO_2)_{140}H_8$ system consisting of two truncated bipyramidal anatase particles attached on (001) or (101) facets. Ti, O, and H atoms are red, gray, and white, respectively. Geometries are optimized using DFT with PBE functional. Figure adapted from reference 23.

Instead we successfully adapted and tested three other methods with increasing levels of sophistication: (a) the semi-empirical density functional tight binding (DFTB) method, (b) DFT under the generalized gradient approximation (GGA), and (c) DFT using a hybrid functional [23]. We found that these methods compare more favorably to the available experimental data. Both types of connected anatase particles have orbitals localized at the interfaces with energies near the edge of the nominal CB (Figure 3). The absolute depth of the trap states is dependent upon calculation method, while the physical orientation of the interface was found to consistently alter the relative depth of the associated trap states independent of calculation method. All three theoretical frameworks predict that the trap states localized at the interface between (001) facets are lower in energy than those localized at the interface between (101) facets [23]. The theoretical insights into the nature of interfacial trapping states could have a profound impact on development of porous networks of nanocrystalline anatase with controlled preferential attachment.

4.2 Generating Plasmonic Carriers

4.2.1 Spectroscopic Determination of Carrier Generation

After establishing how carrier transport and trapping in oxide networks can be modulated to dictate UV-driven photocatalytic activity, we now determine how the oxide networks can be coupled with plasmonic Au nanoparticles to extend the activity of TiO_2 into the visible light region. We performed ultrafast (sub-picosecond) visible pump—infrared (IR) probe time resolved spectroscopy [24] in order to monitor plasmonic carrier generation in TiO_2 aerogels supporting 5 nm diameter Au nanoparticles (Au–TiO_2).

When the plasmon resonance of Au is excited at 500 nm, the Au–TiO_2 aerogels produced CB electrons that are detected with the 5 μm IR probe pulse and undergo a biexponential decay (Figure 4, Scheme 1). The assignment of this transient signal to CB electrons in TiO_2 is corroborated by the fact that this signal is not observed when Au nanoparticles are supported on SiO_2 aerogels (Au–SiO_2). The hot electrons

generated in plasmonic Au nanoparticles do not have sufficient energy to inject into insulating SiO_2, but can inject into the CB of semiconducting TiO_2. The plasmonic origin of the transient CB electron signal is indicated by the fact that when the Au–TiO_2 aerogels are excited with a visible pump at an excitation energy lower than the SPR maximum (750 nm), the transient signal is significantly weaker compared to when the pump energy is ≥ the maximum SPR frequency. The direct observation of CB electron generation in Au–TiO_2 upon visible-light excitation, along with the wavelength dependence of this transient signal, confirms the injection of SPR-generated electrons into the TiO_2 aerogel network.

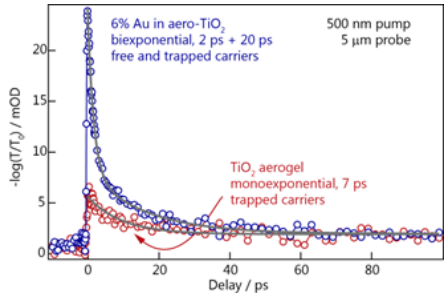

Fig. 4 — Normalized transient-decay curves after excitation with 500 nm pump with probe maintained at 5µm

Although Au-free TiO_2 aerogels also produce a CB electron signal with a visible pulse, the TiO_2 signal is significantly weaker compared to Au–TiO_2 and exhibits single-exponential decay (Figure 4). Since 500 nm excitation is at a lower energy than the anatase TiO_2 bandgap, the excitation of CB electrons in TiO_2 likely derives from the shallow trap states at particle-particle junctions (Figure 3) [22,23]. The substantially higher population of CB electrons produced from Au–TiO_2 relative to TiO_2 indicates that visible-light-driven activity will mostly arise from plasmonically generated carriers as opposed to those generated from shallow trap states in the TiO_2.

4.2.2 Influence of Au||TiO_2 Interface on Carrier Dynamics

We compare ultrafast spectroscopy of carrier decay in two types of TiO_2 aerogels featuring Au nanoparticles: those in which Au is deposited onto a pre-formed TiO_2 aerogel (Au_{ON}/TiO_2) and those in which Au is incorporated into the aerogel network during sol-gel synthesis (Au_{IN}–TiO_2). Both types of composite aerogels produce conduction band electrons upon excitation of the surface plasmon resonance, however, their excited state lifetimes differ (Figure 5). We observe three distinct regimes of carrier dynamics for the composite aerogels: 1) recombination with Au (<10 ps), 2) relaxation into deeper traps (40 ps), and 3) a persistent signal (>1 ns). The Au_{IN}–TiO_2 aerogels have a much higher proportion of fast recombination with Au, courtesy of a more intimate Au||TiO_2 interface. Electrons in Au_{IN}–TiO_2 composites are better able to traverse the aerogel network and recombine with Au nanoparticles compared to the Au_{ON}/TiO_2 composites.

The different excited-state lifetimes for SPR-generated CB electrons suggest distinct electron trapping mechanisms in the two composite aerogels. This result is consistent with the disparate apparent concentrations of electron-trapping surface defects in the two aerogel composites measured both by solid-state nuclear magnetic resonance (NMR) spectroscopy and electron paramagnetic resonance (EPR) spectroscopy, even at relatively low weight fractions of incorporated Au nanoparticles (~1 weight% Au). The convergence of results of the different methods suggests that Au nanoparticles incorporated into TiO_2 aerogels have strong, long-range (10s to 100s of nanometers) effects on both electron mobility and dynamics in the aerogels, and possibly on surface molecular diffusion as well.

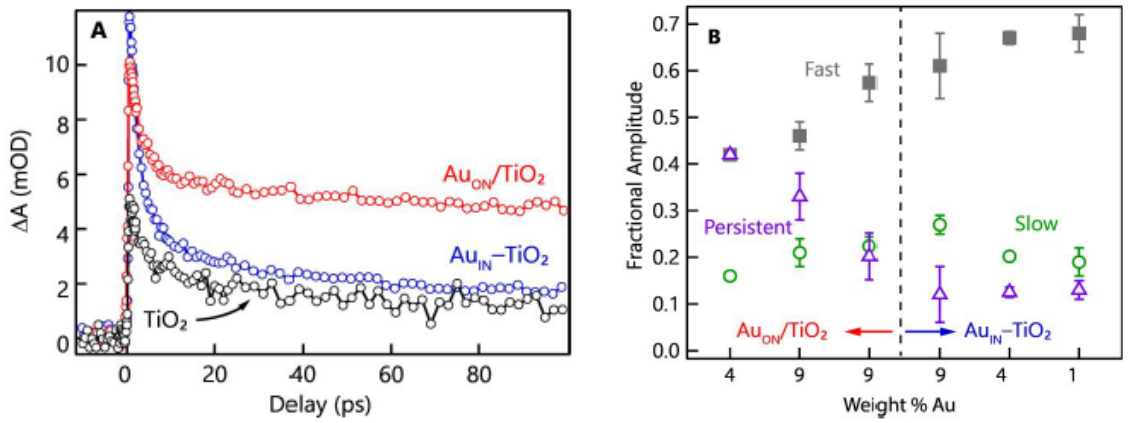

Fig. 5 — (A) Ultrafast transient IR spectroscopy with a 500 nm pump pulse and a 5μm probe pulse showing decay of conduction band elections in composite aerogels when Au is incorporated into sol-gel precursors prior to gelation of the network (Au_{IN}–TiO_2) and when Au is deposited onto a preformed TiO_2 aerogel (Au_{ON}/TiO_2); (B) fractional amplitude of the fast, flow, and persistent components of the transient decay.

4.2.3 Photocatalytic Water Reduction with Plasmonic Carriers – Dual Roles of Au

We determine the cooperative influence of plasmonic sensitization from Au nanoparticles and trapping states at particle—particle junctions in TiO_2 aerogels on photocatalytic H_2 generation under both broadband (UV + visible) and visible-only (>435 nm) excitation [24]. While increasing the number of trap states in TiO_2 alone yields an 8× improvement in surface-area-normalized H_2 generation rate, incorporation of Au nanoparticles into the TiO_2 aerogels improves activity ~50-60× over Au-free TiO_2 (Figure 2A, Figure 6). An additional 2× improvement is realized when Au nanoparticles are incorporated into TiO_2 aerogels with a higher density of electron traps.

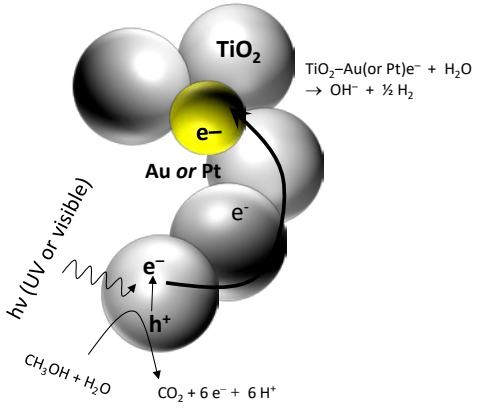

Scheme 2

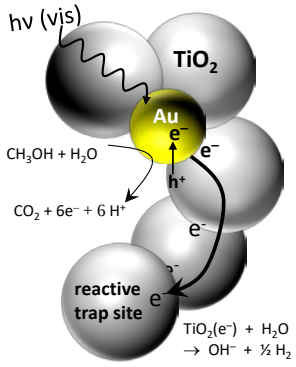

Scheme 3

Under broadband excitation, Au can serve both as a water-reduction catalyst and a plasmonic sensitizer. In the co-catalyst role, carriers generated by excitation of the TiO_2 bandgap can migrate to the Au||TiO_2 interface to reduce water (Scheme 2). Transfer of electrons to Au hinders carrier recombination and at the same time, the Au surface is more active and selective than the TiO_2 surface for water reduction. In the SPR-driven pathway (Scheme 3), hot electrons are injected from Au to the TiO_2 conduction band. The

hole performs oxidation chemistry at the Au||TiO_2 interface while the electron can migrate through the oxide network to catalytically active sites on the TiO_2 surface (i.e. trap sites).

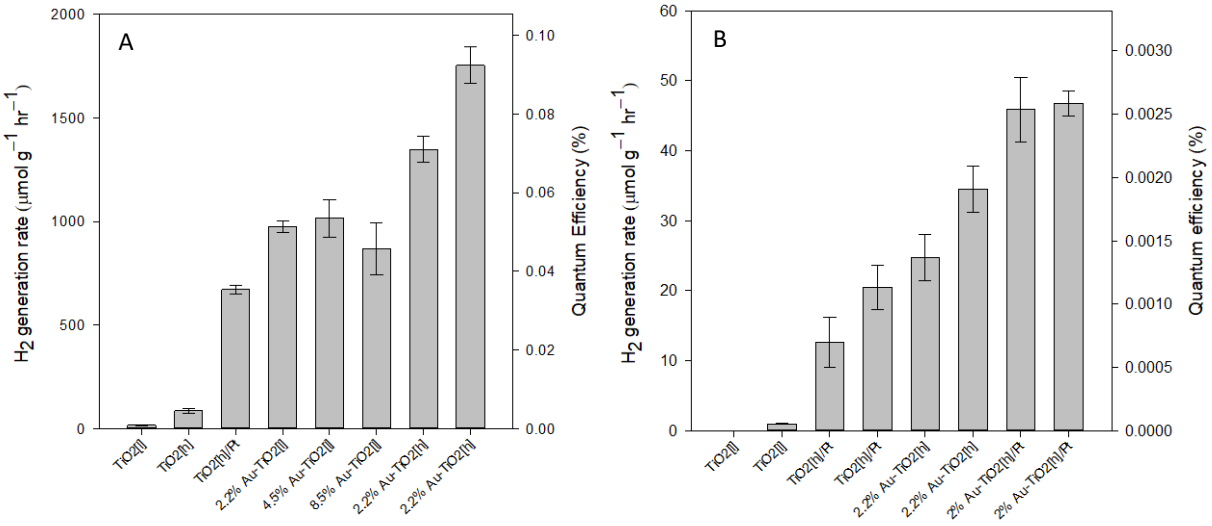

Fig. 6 — Quantum efficiency and mass-normalized rate of photocatalytic hydrogen generation under (A) broadband illumination (UV + visible) and (B) visible illumination (>435 nm). Comparisons are made between TiO_2 aerogels with a high or low network density (denoted TiO_2[h] and TiO_2[l], respectively) with or without plasmonic Au nanoparticles (denoted Au–TiO_2) and composite aerogels containing plasmonic Au nanoparticles and with Pt nanoparticles deposited on the composite aerogel (denoted Au–TiO_2/Pt). Figure adapted from reference 24.

The SPR-driven pathway is less prominent than the former pathway under broadband illumination evidenced by the fast that the mass-normalized rate of H_2 generation under visible illumination (when only the SPR-driven pathway is functional) is 40-60× lower than under broadband illumination (Figure 6). Even at sub-bandgap excitation, the Au-free TiO_2 aerogel shows a minimal amount of H_2 generation due to excitation of carriers from shallow traps. The majority of visible-light-driven photocatalysis in Au/TiO_2 aerogels is, however, attributed to plasmonically generated carriers, consistent with the order of magnitude higher H_2 generation rate and more intense transient IR signal observed for Au/TiO_2 relative to TiO_2.

4.2.4 Effect of Au size on Plasmonic Sensitization

After demonstrating that plasmonic carriers can be injected from Au into the TiO_2 CB (Scheme 1) and subsequently transported to trap sites to perform photochemistry (Figure 6), we then determine how Au diameter dictates the quantum efficiency for plasmon-enhanced photochemistry. Larger diameter Au nanoparticles are entrained in TiO_2 aerogels by inclusion of polymer stabilized Au NPs in the gelation solution. While our alkane-thiol stabilized Au nanoparticles are limited to a size of 5 nm, the polymer-stabilized method provides considerably more flexibility for the inclusion of Au NPs of a variety of sizes. We entrain 15 nm Au NPs in TiO_2 aerogels to determine the impact of Au diameter on catalyst performance in photochemical hydroxide and methoxide oxidation.

The SPR of the 15 nm diameter particles is significantly more intense than that of the 5 nm diameter particles at the same Au weight loading in TiO_2 aerogels (Figure 7A). The larger Au NPs also display considerably improved performance for photochemical oxidation of hydroxide and methanol (Figure 7B). Despite a fewer total number of Au particles at the larger diameter, on a per mass basis, the larger particles are a more efficient utilization of Au.

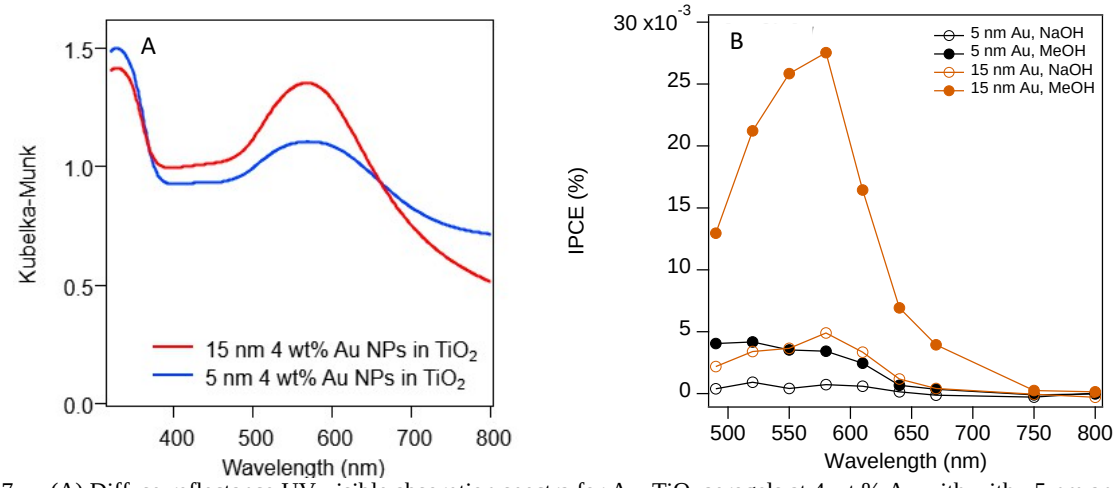

Fig. 7 — (A) Diffuse-reflectance UV-visible absorption spectra for Au–TiO_2 aerogels at 4 wt.% Au with with ~5 nm and ~15 nm diameter Au nanoparticles; (B) incident photon-to-current efficiency for 4 wt.% Au with with ~5 nm and ~15 nm diameter Au nanoparticles in 0.1 M NaOH solutions (open circles) and 0.5 M Methanol/0.1M NaOH (closed circles)

4.3 Wiring Plasmonic Carriers to Co-catalysts through the Oxide Network

Regardless of if photogenerated electrons in TiO_2 originate from bandgap excitation, shallow trap excitation, or injection from a plasmonic sensitizer, their efficient utilization is ultimately dependent upon their transfer to a surface site that is active and selective for the reaction of interest. In other words, TiO_2 can provide adequate thermodynamic potentials to drive chemical reactions of interest, but how can we improve kinetics? While we have demonstrated excitation of carriers from plasmonic Au into the TiO_2 network, wiring the plasmonically generated carriers to another co-catalyst can ultimately improve the utilization of SPR-generated charge carriers.

We introduce non-plasmonic Pt co-catalyst nanoparticles into our composite aerogels (Au–TiO_2/Pt) in order to leverage the catalytic water-reducing abilities of Pt and demonstrate electrochemical linkage of the SPR-generated carriers at the Au||TiO_2 interfaces to downfield Pt nanoparticle co-catalysts [24]. The Au–TiO_2/Pt aerogels are synthesized by photodepositing ~2-nm diameter Pt nanoparticles at preformed 3D Au–TiO_2 aerogels under visible illumination. By using SPR-generated carriers to execute reductive photodeposition of the Pt nanoparticles we preferentially deposit Pt at trapping sites electronically wired to plasmonic sensitizers. When Pt is incorporated into Au–TiO_2, H_2 generation activity under visible illumination improves by ~2× (Figure 6B, Figure 8), confirming that electrons generated by excitation of the Au SPR are wired through the TiO_2 network to the Pt nanoparticles.

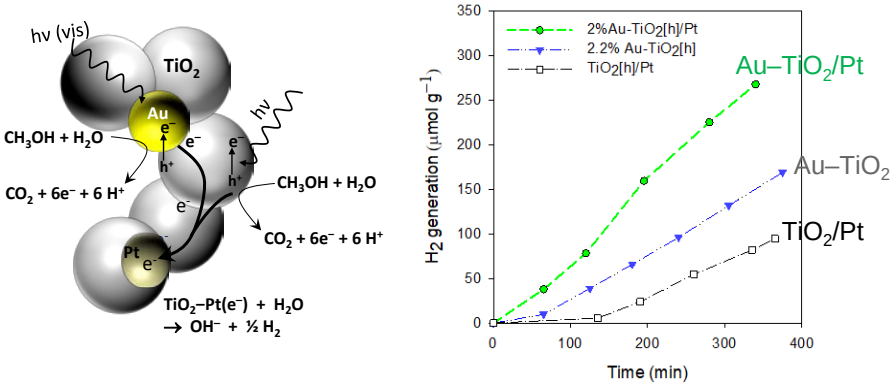

Fig. 8 — Schematic of charge transfer in composite Au—TiO_2/Pt catalyst (left panel) and mass-normalized rate of photocatalytic hydrogen generation over Au–TiO_2 /Pt, Au–TiO_2, and TiO_2/Pt aerogels under visible illumination (>435 nm).

The Au–TiO_2/Pt arrangement in three dimensions effectively utilizes conduction band electrons injected into the TiO_2 aerogel network upon excitement of the Au SPR at the Au||TiO_2 interface. The extensive nanostructured high surface-area network in the aerogel provides a matrix that spatially separates while electrochemically connecting plasmonic nanoparticle sensitizers and metal nanoparticle catalysts, further enhancing solar fuels photochemistry. Additionally, these visible-light H_2 -generation photocatalytic data comprise concrete proof that the plasmonic Au||TiO_2 interface can be wired to a separate reduction catalyst within the same composite aerogel. Thus, Au–TiO_2/Pt the aerogel comprises a stable, visible light–active photocatalytic architecture that enables photocatalytic generation of hydrogen (H_2) fuel using only renewable feedstocks such as alcohols or water.

Analogous to utilizing Pt as a reduction catalyst, we similarly anchor Iridium Oxide (IrO*x*) nanoparticles on the composite aerogels to more efficiently utilize photogenerated holes for oxidation (i.e. improve the kinetics of water oxidation). We chose IrO*x* because it is one of the best known water oxidation catalysts, but in order to leverage this activity, it must be wired to photogenerated holes in Au/TiO_2 aerogels. Holes are significantly less mobile than electrons in TiO_2, and we have previously determined that hole-mediated chemistry occurs locally at the Au||TiO_2 interface [25]. Thus, we target the incorporation IrO*x* nanoparticles at the Au||TiO_2 interface or directly at the surface of Au nanoparticles. We initially attempted to photo-deposit IrO*x* on Au nanoparticles, however, the oxidative potential supplied by the Au SPR was insufficient to photodeposit IrO*x*. Instead we link IrO*x* nanoparticles to the Au via the thiol group of 3-mercaptopropionic acid. The photoelectrochemical activity of Au–TiO_2 aerogels was improved by a factor of 10× when IrO*x* nanoparticles were in contact with Au, however, we have not yet determined how stable the ligand-tethered particles are during this reaction.

4.4 Plasmonic Cu as a non-precious alternative to Au

4.4.1 Stabilizing Plasmonic Cu Nanoparticles on TiO_2 Aerogel Supports

Stabilization of Cu in its primary metallic and plasmonic form under operando conditions is challenging [26], therefore, SPR-enhanced photocatalysts has almost exclusively been limited to using either plasmonic Au or Ag. The scarce reports describing plasmonic applications of Cu convey the necessity of maintaining Cu in anoxic environments or encapsulating the particles to inhibit oxidation [27,28,29,30,31,32]. We demonstrate that the SPR of Cu nanoparticles is stabilized by offering an extended interfacial contact with a reducing metal oxide support, i.e. TiO_2 aerogels [33].

The Cu/TiO_2 aerogels are synthesized by photodepositing < 5-nm Cu nanoparticles at pre-formed TiO_2 aerogels [33]. The extended nanoscale Cu||TiO_2 junctions in composite aerogels stabilize Cu against oxidation to an extent that preserves the plasmonic behavior of the nanoparticles, even after exposure to oxidizing conditions (Figure 9). In contrast, photoreduction of Cu(II) at a commercial nanoscale anatase TiO_2 powder with primary particle sizes significantly larger than those in the aerogel results in a copper oxide/TiO_2 composite that exhibits none of the plasmonic character of metallic Cu nanoparticles.

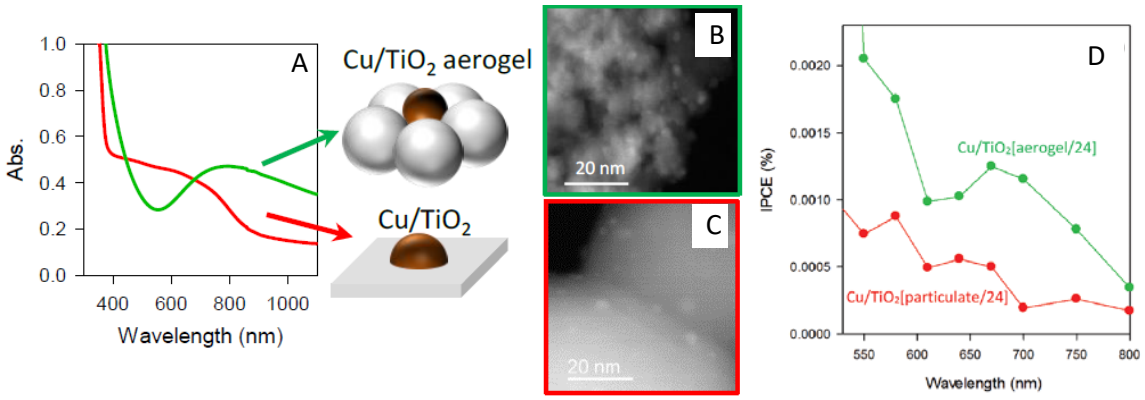

Fig. 9 — (A) Diffuse-reflectance UV-visible absorption spectra for Cu nanoparticles deposited on TiO_2 aerogels (Cu/TiO_2 aerogel) or commercial anatase TiO_2 nanoparticles (Cu/TiO_2 nanoparticulate); scanning electron micrographs of (B) Cu/TiO_2 aerogel and (C) Cu/TiO_2; (D) photocurrent action spectrum for incident photon conversion efficiency in alcohol/water solution at photoanodes derived from Cu/TiO_2 aerogels and Cu/TiO_2 nanoparticulate. Figure adapted from reference [33].

We attribute the stabilization of plasmonic Cu nanoparticles without the use of ligand stabilizers to the arrangement of Cu and TiO_2 within the aerogel architecture where each Cu nanoparticle is in contact with multiple nanoparticles of reducing oxide. The wavelength dependence of the photoaction spectra for Cu/TiO_2 aerogel films (Figure 9) reveals visible-light photocatalytic oxidation activity initiated by an SPR-driven process—as opposed to photo-oxidation initiated by excitation of narrow-bandgap copper oxides [33]. The stabilization of Cu nanoparticles in primarily metallic form at oxide-based supports without ligand stabilizers is to date unique to the Cu TiO_2 aerogel architecture.

4.4.2 Small Molecule Oxidation at Cu/TiO_2 Aerogels

We determine how the oxidation state of supported Cu particles—as influenced by its interfacial arrangement with TiO_2–impacts oxidative activity for thermal catalysis [34]. Low-temperature CO oxidation is chosen as a probe reaction for the general oxidative activity of Cu nanoparticles because the linkage between CO oxidation activity and Cu oxidation state are well characterized. This reaction also allows us to characterize the stability of Cu nanoparticles on TiO_2 aerogel supports under practical conditions (i.e. aerobic atmosphere and elevated temperatures) and to establish baseline levels of thermal catalysis that can be subsequently compared to photocatalysis.

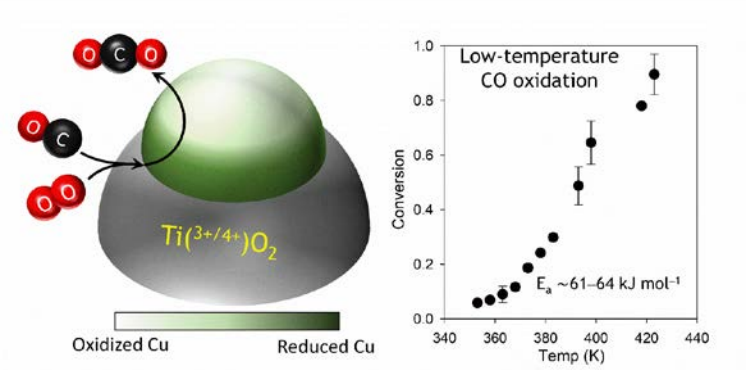

Fig. 10 — Fractional conversion of CO vs. temperature for Cu/TiO_2 aerogels in a continuous plug flow reactor. Activation energy is calculated from Arrhenius plots made using data at 3-15% conversion of CO to CO_2.

The Cu/TiO_2 aerogels are highly active for low-temperature oxidation of CO and are more active than Cu on commercial anatase supports. The $Cu^{0/1+}$ speciation stabilized within the aerogel catalyzes low-temperature CO oxidation (< 100 °C) at high conversion rates and does not necessitate high temperature activation in a reducing gas stream (Figure 10)—performance that the non-networked catalyst cannot meet [34]. The multiple points of contact between supported Cu nanoparticles and the ~10-nm particles of the aerogel facilitate donation of electron density from the reducing oxide to the supported Cu nanoparticles. More usefully, Cu/aerogels do not require strict UHV environments or an aggressive reduction step in order to retain the reduced forms of Cu needed to exhibit high rates of CO conversion at low temperature.

Although Cu/TiO_2 aerogels are not as active as Au/TiO_2 aerogels for low-temperature CO oxidation, the initial demonstration of the catalytic stability and oxidative activity at Cu/TiO_2 aerogels has paved the way for different applications. Notably, the Cu/TiO_2 aerogels have since been demonstrated to be efficient catalysts for degradation of organophosphorus chemical warfare simulants and agents in an externally funded program. While Au is still the better small molecule oxidation catalyst compared to Cu, Cu has consistently shown superior activity for Au for degradation of organophosphorus compounds where both hydrolytic and oxidative degradation pathways are important.

5. CONCLUSIONS

The TiO_2 aerogel architecture enables modification of multiple functional parts of the integrated composite photocatalyst. Sensitizing TiO_2 aerogels with Au nanoparticles enables visible-light SPR-driven photocatalytic water splitting. Although some visible-light H_2 generation is observed with bare TiO_2 aerogels, plasmonic carriers account for the overwhelming majority of visible-light initiated photocatalysis. The visible-light-driven activity in Au-free TiO_2 is due to excitation from shallow trap states residing at particle-particle junctions. The energies and locations of the trap states were predicted with first principles calculations and their impact on carrier transport and trapping was experimentally characterized by transient photoelectrochemical techniques. The fate of plasmonically-generated carriers is highly dependent upon the $Au||TiO_2$ interfacial density. When coupled with synthetically integrated trap states at particle-particle junctions of the oxide, SPR-derived carriers show improved activity for H_2 generation relative to composite aerogels with a smaller population of trap states. More efficient carrier generation could be accomplished with larger diameter Au nanoparticles relative to smaller diameter particles.

While TiO_2 surfaces are non-selective for both water reduction and water oxidation, wiring plasmonic carriers to a co-catalyst can improve photoactivity. Incorporating Pt at electron trap sites or IrO_2 at hole trap sites improve water reduction and water oxidation, respectively. Plasmonic sensitization of TiO_2 aerogels was also demonstrated with Cu nanoparticles. The Cu nanoparticles could be maintained in persistent, low-valent state courtesy of charge transfer at the extended $Cu||TiO_2$ interface which preserves their plasmonic activity. The interfacial arrangement stabilizes the low-valent, and more oxidatively active form of Cu which has been demonstrated for small molecule oxidation (CO oxidation) and degradation of organophosphorus compounds.

The fundamental insights gained in this program spurred two externally funded programs stemming from this seminal work, each focusing on a different application for plasmonic photocatalysts. A research program was sponsored in order to focus specifically on tailoring the activity of plasmonic photocatalsts for H_2 generation from water. Another program was funded to focus solely on the degradation of organophosphorus compounds using non-precious-metal plasmonic sensitizers. Each of those programs

have built upon the foundation of knowledge laid by our initial investigations into 3D Nanostructured Photocatalysis.

6. PRODUCTIVITY

6.1 Publications

6.1.1 Peer-reviewed journal publications

1. P. A. DeSario, C.L. Pitman, D.J. Delia, D.R. Rolison, J.J. Pietron, (2019) "Low-temperature CO oxidation at persistent low-valent Cu nanoparticles on TiO_2 aerogels," *Appl. Catal. B*, 252, 205–213.
2. N.Q. Le, C.E. Ekuma, B.I. Dunlap,D. Gunlycke, D., (2018) "First-Principles Calculations of Sarin Adsoprtion on Anatase Surfaces," *J. Phys. Chem. C*, 122, 2832–2839.
3. P.A. DeSario, J.J. Pietron, T.H. Brintlinger, J.F. Parker, O. Baturina, R.M. Stroud, D.R. Rolison (2017) "Oxidation-stable plasmonic copper nanoparticles in photocatalytic TiO_2 nanoarchitectures," *Nanoscale*, 9, 11720–11729.
4. **INVITED**: P.A. DeSario, J.J. Pietron, A. Dunkelberger, T.H. Brintlinger, O. Baturina, R.M. Stroud, J.C. Owrutsky, D.R. Rolison, (2017) "Plasmonic aerogels as a three-dimensional nanoscale platform for solar fuels photocatalysis," *Langmuir*, 33, 9444–9454, special issue on "Fundamental Interfacial Science for Energy Applications."
5. **INVITED**: J.J. Pietron, P.A. DeSario, (2017) "Roles for Photonic Crystals in Solar Fuels Photocatalysis," *Journal of Photonics for Energy*, 7(1), 012007.
6. N.Q. Le, I.V. Schweigert, (2017) "Modeling Electronic Trap States at Interfaces Between Anatase Nanoparticles," *J. Phys. Chem. C*, 121, 14254–14260.
7. I.V. Schweigert, D. J. Gunlycke, (2017) "Hydrolysis of Dimethyl Methylphosphonate by the Cyclic Tetramer of Zirconium Hydroxide," *J. Phys. Chem. A*, 121, 7690.
8. **INVITED**: Z. H. Kafafi,* R. J. Martín-Palma, A. F. Nogueira, D. M. O' Carroll, J. J. Pietron,* I. D. W. Samuel, F. So, N. Tansu, and L. Tsakalakos, (2015) "Role of photonics in energy," *Journal of Photonics for Energy*, 5, 050997.
9. P.A. DeSario, J.J. Pietron, D.H. Taffa, R. Compton, S. Schuenemann, M. Roland, T.H. Brintlinger, R.M. Stroud, M. Wark, J.C. Owrutsky, D.R. Rolison (2015) "Correlating changes in electron lifetime and mobility on photocatalytic activity at network-modified TiO_2 aerogels," *J. Phys. Chem. C*, 119, 17529–17538.

6.1.2 Conference proceedings

10. T.H. Brintlinger, P.A. DeSario, J.J. Pietron, R.M. Stroud, D.R. Rolison (2016) "Aberration-corrected Scanning Transmission Electron Microscopy and Spectroscopy of Nonprecious Metal Nanoparticles in Titania Aerogels," *Microscopy and Microanalysis*, 22(3), 324–326.

6.2 Presentations

1. "Nanoscale Modification of Plasmonic Aerogels for Photocatalytic H_2 Generation," Pitman, C. L., Pietron, J. J.; DeSario, P. A.; Dunkelberger, A.; Brintlinger, T. H.; Owrutsky, J. C.; Stroud, R. M.; Rolison, D. R. *Spring Meeting of the Materials Research Society*, Phoenix, AZ, April 22–26, 2019.
2. **INVITED**: "Stabilization and Reactivity of Low-Valent Copper on Titania Aerogels." Pitman, C. L.; Pennington, A. M.; Delia, D. J.; DeSario, P. A.; Rolison, D. R.; Pietron, J. J.; McEntee,

M. L.; Balboa, A.; Gordon, W. O. *Gordon Research Seminar on Metal-Based Reactions for Sustainability*, Galveston, TX, March 9–10, 2019.

3. "Stabilization and Reactivity of Low-Valent Copper on Titania Aerogels." Pitman, C. L.; Pennington, A. M.; Delia, D. J.; DeSario, P. A.; Rolison, D. R.; Pietron, J. J.; McEntee, M. L.; Balboa, A.; Gordon, W. O. *Gordon Research Conference on Metal-Based Reactions for Sustainability*, Galveston, TX, March 10–15, 2019.
4. "Promoting Solar-Driven Water Splitting on Au–TiO_2 Aerogels," Pitman, C. L.; DeSario, P. A.; Pietron, J. J.; Rolison, D. R. *Conference on Status and Challenges in Science for Decarbonizing our Energy Landscape*, Beckman Center, Irvine, CA, October 10–12, 2018.
5. **INVITED**: "Nanoscale Design and Modification of Plasmonic Aerogels for Photocatalytic Hydrogen Generation." J. J. Pietron, P. A. DeSario, C. L. Pitman, T. H. Brintlinger, A. Dunkelberger, O. Baturina, R. M. Stroud, J. C. Owrutsky, D. R. Rolison, *233rd Meeting of the Electrochemical Society*, Seattle, WA, 13–17 May 2018.
6. **INVITED**: "Oxidation-stable plasmonic copper nanoparticles in catalytic TiO_2 aerogels," P.A. DeSario, J.J. Pietron, T.H. Brintlinger, J.F. Parker, O.A. Baturina, R.M. Stroud, and D.R. Rolison, *255th ACS National Meeting and Exposition*, New Orleans, LA, 18–22 March 2018.
7. "Photocatalytic hydrogen generation activity at plasmonic Au–TiO_2 and Au–TiO_2/Pt aerogels," J. J. Pietron, P. A. DeSario, C. L. Pitman, T. H. Brintlinger, A. Dunkelberger, O. Baturina, R. M. Stroud, J. C. Owrutsky, D. R. Rolison, *255th ACS National Meeting & Exposition*, New Orleans, LA, 18–22 March, 2018.
8. **INVITED:** "Plasmonic photocatalysis and small molecule oxidation catalysis at oxidation-stable Cu–TiO_2 aerogels," J.J. Pietron, P.A. DeSario, D.J. Delia, D.R. Rolison, T.H. Brintlinger, M. McEntee, *255th Symposium on Nanomaterials for Environmental Purification and Energy Conversion*, Institute for Catalysis, Hokkaido University, Sapporo, Japan, 20–21 February 2018.
9. "Oxidation-Stable Plasmonic Copper Nanoparticles in Photocatalytic TiO_2 Nanoarchitectures," P. A. DeSario, J. J. Pietron, T. H. Brintlinger J. F. Parker, O. Baturina, R. M. Stroud, and D. R.Rolison, *232nd Meeting of the Electrochemical Society*, 1–6 October 2017, National Harbor, MD.
10. "Wiring a Mesoscale Catalytic Architecture for Solar Fuels Production," J. J. Pietron, P. A. DeSario, A, Dunkelberger, T. H. Brintlinger, J. C. Owrutsky, and D. R. Rolison, *232nd Meeting of the Electrochemical Society*, 1–6 October 2017, National Harbor, MD.
11. "Effects of Nanoscale Interfacial Design on Photocatalytic Hydrogen Generation Activity at Plasmonic Au–TiO_2 and Au–TiO_2/Pt Aerogels." J. J. Pietron, P. A. DeSario, T. H. Brintlinger, O. A. Baturina, R. M. Stroud, and D. R. Rolison, *232nd Meeting of the Electrochemical Society*, National Harbor, MD, 1–5 October 2017.
12. "Oxidation-stable plasmonic copper nanoparticles in photocatalytic TiO_2 aerogels." J. J. Pietron, P. A. DeSario, J. F. Parker, D. R. Rolison, O. Baturina, T. H. Brintlinger, R. M. Stroud, *6th International Conference on Semiconductor Photochemistry*, Oldenburg, Germany, 11–14 September 2017.
13. "Photocatalytic H_2 generation at plasmonic Au–TiO_2 and Au–TiO_2/Pt aerogels: Effects of nanoscale interfacial design." J. J. Pietron, P. A. DeSario, D. R. Rolison, A. Dunkelberger, J. C. Owrutsky, O. Baturina, T. H. Brintlinger, and R. M. Stroud, *6th International Conference on Semiconductor Photochemistry*, Oldenburg, Germany, 11–14 September 2017.
14. **INVITED**: "Effects of nanoscale interfacial design on the UV and visible photocatalytic activity of plasmonic aerogels." J. J. Pietron, P. A. DeSario, T. H. Brintlinger, R. M. Stroud, and D. R. Rolison, *253rd Meeting of the American Chemical Society*, San Francisco, CA, 2–6

April 2017.

15. "Effects of interfacial design in Au–TiO_2 and Cu–TiO_2 plasmonic aerogels for visible light–driven photocatalysis." D. R. Rolison, P. A. DeSario, J. J. Pietron, E. R. Glaser, J. P. Yesinowski, T. H. Brintlinger, R. M. Stroud, *Spring Meeting of the Materials Research Society*, Phoenix, AZ, 17–21 April 2017.
16. **INVITED:** "Modeling electronic trap state distributions in nanocrystalline anatase", Le, N.Q. and Schweigert, I.V., *American Physical Society March Meeting*, March 2017, New Orleans, Louisiana.
17. "Modeling TiO_2 aerogels: from nanoparticles to networks." N.Q. Le, I. Schweigert, *252nd American Chemical Society Meeting*, 21-25 August 2016, Philadelphia, PA.
18. **INVITED**: "Oxidative photocatalysis at TiO_2 aerogels driven by surface plasmon resonance of non-precious metal nanoparticles." J. J. Pietron, P. A. DeSario, T. H. Brintlinger, R. M. Stroud, and D. R. Rolison, *DTRA Review of Surface Science and Multifunctional Materials for Protection*, Raleigh, NC, 27–29 September 2016.
19. "Aberration-corrected scanning transmission electron microscopy and spectroscopy of nonprecious metal nanoparticles in titania aerogels." T. H. Brintlinger, P. A. DeSario, J. J. Pietron, R. M. Stroud, and D. R. Rolison, *2016 Microscopy & Microanalysis*, Columbus, OH, 24–28 July 2016.
20. "Modeling Interfacial Trap States in Anatase Nanoparticles," N. Le, I. Schweigert, *Gordon Research Conference on Molecular Interactions and Dynamics*, Easton, MA, 9–10 July 2016.
21. **INVITED**: "Oxidative photocatalysis at TiO_2 aerogels driven by surface plasmon resonance of gold and nonprecious metal nanoparticles." J. J. Pietron, P. A. DeSario, T. H. Brintlinger, R. M. Stroud, and D. R. Rolison, *90th ACS Colloid & Surface Science Symposium*, Cambridge, MA, 5–8 June 2016.
22. **INVITED**: "Designing catalytic nanoarchitectures for efficient photochemical and photoelectrochemical water-splitting," P. A. DeSario, J. J. Pietron, A. D. Dunkelberger, C. N. Chervin, J. C. Owrutsky, and D. R. Rolison, McCormick School of Engineering Lecture Symposium, Northwestern University, Evanston, IL, 13 May 2016.
23. "Oxidative photocatalysis at TiO_2 aerogels driven by surface plasmon resonance of non-precious metal nanoparticles." P. A. DeSario, J. J. Pietron, T. H. Brintlinger, R. M. Stroud, and D. R. Rolison, *Spring Meeting of the Materials Research Society*, Phoenix, AZ, 28 March–1 April 2016.
24. "Aberration-corrected scanning transmission microscopy investigation of non-precious metal nanoparticulate guests hosted within titania aerogels." T. H. Brintlinger, P. A. DeSario, J. J. Pietron, R. M. Stroud, and D. R. Rolison, *Spring Meeting of the Materials Research Society*, Phoenix, AZ, 28 March–1 April 2016.
25. "Designing composite Au–TiO_2 aerogels for UV- and visible-light photocatalytic water splitting: Effects of Au||TiO_2 interfacial design at the nanoscale." J. J. Pietron, P. A. DeSario, T. H. Brintlinger, R. Compton, J. C. Owrutsky, and D. R. Rolison, *Spring Meeting of the Materials Research Society*, Phoenix, AZ, 28 March–1 April 2016.
26. "Effects of modifying nanoscale interconnects in TiO_2 aerogels on electron lifetimes and mobility: Consequences for reductive and oxidative photocatalytic activity." J. J. Pietron, P. A. DeSario, D. H. Taffa, R. Marschall, S. Schünemann, M. Wark, R. Compton, J. C. Owrutsky, and D. R. Rolison, *Spring Meeting of the Materials Research Society*, Phoenix, AZ, 28 March–1 April 2016.
27. **Invited**: "Effects of nanoscale network modification and Au||TiO_2 interfacial structure on photochemical and photoelectrochemical activity at composite Au–TiO_2 aerogels." J. J.

Pietron, P. A. DeSario, D. H. Taffa, M. Wark, T. H. Brintlinger, R. M. Stroud, D. R. Rolison , NRL Chemistry Division Meeting with ONR-Global, Washington, DC, 6 January 2016

28. **INVITED**: "Effects of nanoscale network modification and Au||TiO_2 interfacial structure on photochemical and photoelectrochemical activity at composite Au–TiO_2 aerogels," J. J. Pietron, P. A. DeSario, D. H. Taffa, M. Wark, D. A. Panayotov, J. R. Morris, T. H. Brintlinger, R. M. Stroud, and D. R. Rolison, Departmental Seminar in the Laboratory of Industrial Chemistry, Carl von Ossietzky University-Oldenburg, Oldenburg, Germany, 14 December 2015.
29. **INVITED**: "Plasmonic aerogels for photocatalysis: fundamentals, photocatalytic generation of fuels, and decontamination,"J. J. Pietron, P. A.DeSario, D. A.Panayotov, J. R. Morris, T. H.Brintlinger, R. M. Stroud, J. C.Owrutsky, R. Compton, D. E.DeVantier, D. R. Rolison, and W. R.Gordon, presentation at Edgewood Chemical Biological Center, Edgewood, MD, 14 October 2015.
30. **INVITED**: "Plasmonic aerogels for catalytic oxidation." J. Pietron, P. DeSario, D. Panayotov, J. Morris, T. Brintlinger, R. Stroud, D. DeVantier, D. Rolison, and W. Gordon, *Multifunctional Materials for Force Protection Working Group Meeting (DTRA and ECBC)*, Annapolis Junction, MD, 15–16 September 2015
31. **INVITED**: "Designing nanostructured photocatalysts and electrocatalysts for efficient water-splitting." P. A. DeSario, J. J. Pietron, C. N. Chervin, D. R. Rolison, Department of Civil and Environmental Engineering, Lehigh University, Bethlehem, PA, 26 February 2015.
32. "Effects of nanoscale interconnects on electron lifetimes and photocatalytic activity at network-modified TiO_2 aerogels." J. J. Pietron, P. A. DeSario, D. Taffac, R. Marschall, S. Schünemann, M. Wark, R. E. Compton, J. C. Owrutsky, and D. R. Rolison, *Fall Meeting of the Materials Research Society*, Boston, MA, 30 November–5 December 2014.
33. "Effects of nanoscale Au||TiO_2 interfacial structure on SPR-driven photocatalytic activity in Au–TiO_2 aerogels." P. A. DeSario, J. J. Pietron, T. H. Brintlinger, R. M. Stroud, R. E. Compton, J. C. Owrutsky, and D. R. Rolison, *Fall Meeting of the Materials Research Society*, Boston, MA, 30 November–5 December 2014.

6.3 Tech Transfer

1. Invention Disclosure: "Oxidation-stable plasmonic copper nanoparticle–titania composite catalytic nanoarchitectures." J. J. Pietron, P. A. DeSario, D. R. Rolison, T. H. Brintlinger, and R. M. Stroud, 15 March 2016 [Navy Case #104,560].
2. Provisional Patent Application: "Oxidation-stable plasmonic copper nanoparticle–titania composite catalytic nanoarchitectures." J. J. Pietron, P. A. DeSario, D. R. Rolison, T. H. Brintlinger, and R. M. Stroud, 29 March 2016 [Navy Case #104,560].
3. Patent Application (S/N 15/472,782): "Oxidation-stable plasmonic copper nanoparticle–titania composite catalytic nanoarchitectures." J. J. Pietron, P. A. DeSario, D. R. Rolison, T. H. Brintlinger, and R. M. Stroud, 29 March 2017 [Navy Case #104,506].
4. NRL Invention Award, 26 July 2017, "Oxidation-stable plasmonic copper nanoparticle–titania composite catalytic nanoarchitectures," patent application filed for 104056-US2.
5. Foreign Patent Application (104,506-EP; 6 August 2018): "Oxidation-stable plasmonic copper nanoparticle–titania composite catalytic nanoarchitectures." J. J. Pietron, P. A. DeSario, D. R. Rolison, T. H. Brintlinger, and R. M. Stroud [Navy Case #104,506; US patent application S/N 15/472,782].

6.4 Transitions

1. ONR 6.2 Program: “3D nanostructured plasmonic photocatalysts for hydrogen generation from water”—$750k in FY15
2. DTRA 6.1 Program: “Plasmonic Cu nanoparticles on networked mesoporous oxide supports for sunlight-assisted decomposition of CW simulants and live agents”—$281k (3/4 year budget) in FY16 ($142.5k to 6171); $382k in FY17; $390k in FY18

ACKNOWLEDGEMENTS

We would like to acknowledge the following team members on this program:

- PI: Dr. Jeremy Pietron, formerly code 6171
- Dr. Jeffrey Owrutsky, code 6111
- Dr. Igor Schweigert, code 6189
- Dr. Paul DeSario, code 6171

We would like to acknowledge the following collaborators and postdoctoral associates at the U.S. NRL for their contributions to this program:

- Dr. Debra Rolison, code 6171
- Dr. Catherine Pitman, NRC Postdoctoral Associate (current)
- Dr. Ryan Compton, former NRC Postdoctoral Associate
- Dr. Adam Dunkelberger, code 6111
- Dr. Todd Brintlinger, code 6366
- Dr. Rhonda Stroud, code 6366
- Dr. Nam Le, former NRC Postdoctoral Associate
- Dr. Olga Baturina, code 6134
- Daniel Delia, former Pathways Student, U.S. Naval Research Laboratory
- Devyn Devantier, former Pathways Student, U.S. Naval Research Laboratory
- Dr. Joseph Parker, code 6171

Finally, we could like to acknowledge our external collaborators:

- Prof. Michael Wark, Ruhr-University Bochum, Bochum Germany
- Prof. John R. Morris, Virginia Tech, Blacksburg, VA
- Dr. Monica McEntee, U.S. Army Combat Capabilities Development Command Chemical Biological Center

REFERENCES

1. A. Fujishima and K. Honda, *Nature*, 1972, **238**, 37–38.

2. A. Furube, L. Du, K. Hara, R. Katoh and M. Tachiya, *J. Am. Chem. Soc.*, 2007, **129**, 14852–14853.

3. S. Link, Z. L. Wang and M. A. El-Sayed, *J. Phys. Chem. B*, 1999, **103**, 3529–3533.

4. U. Kreibig and M. Vollmer, *Optical Properties of Metal Clusters*, Springer, 1995.

5. S. Link and M. A. El-Sayed, *Int. Rev. Phys. Chem.*, 2000, **19**, 409–453.

6. S. Link and M. A. El-Sayed, *J. Phys. Chem. B*, 1999, **103**, 4212–4217.

7. J. J. Pietron, R. M. Stroud and D. R. Rolison, *Nano Lett.*, 2002, **2**, 545–549.

8. N. Hüsing and U. Schubert, *Angew. Chem., Int. Ed.*, 1998, **37**, 23–45.

9. N. Leventis, I. A. Elder, D. R. Rolison, M. L. Anderson and C. I. Merzbacher, *Chem. Mater.*, 1999, **11**, 2837–2845.

10. M. S. Doescher, J. J. Pietron, B. M. Dening, J. W. Long, C. P. Rhodes, C. A. Edmondson and D. R. Rolison, *Anal. Chem.*, 2005, **77**, 7924–7932.

11. C. Laberty-Robert, J. W. Long, K. A. Pettigrew, R. M. Stroud and D. R. Rolison, *Adv. Mater.*, 2007, **19**, 1734–1739.

12. D. R. Rolison, *Science*, 2003, **299**, 1698–1701.

13. G. Dagan and M. Tomkiewicz, *J. Non-Cryst. Solids*, 1994, **175**, 294–302.

14. M. L. Anderson, R. M. Stroud, C. A. Morris, C. I. Merzbacher and D. R. Rolison, *Adv. Eng. Mater.*, 2000, **2**, 481–488.

15. J. J. Pietron, A. M. Stux, R. S. Compton and D. R. Rolison, *Sol. Energy Mater. Sol. Cells*, 2007, **91**, 1066–1074.

16. Á. Valdés, J. Brillet, M. Grätzel, H. Gudmundsdóttir, H. A. Hansen, H. Jónsson, P. Klüpfel, G.-J. Kroes, F. Le Formal, I. C. Man, R. S. Martins, J. K. Nørskov, J. Rossmeisl, K. Sivula, A. Vojvodic and M. Zäch, *Phys. Chem. Chem. Phys.*, 2012, **14**, 49–70.

17. M. G. Walter, E. L. Warren, J. R. McKone, S. W. Boettcher, Q. X. Mi, E. A. Santori and N. S. Lewis, *Chem. Rev.*, 2010, **110**, 6446–6473.

18. P.A. DeSario, J.J. Pietron, D.E. DeVantier, T.H. Brintlinger, D.R. Rolison, *Nanoscale*, 2013, **5**, 8073–8083.

19. C. A. Morris, M. L. Anderson, R. M. Stroud, C. I. Merzbacher and D. R. Rolison, *Science*, 1999, **284**, 622–624.

20. M. L. Anderson, C. A. Morris, R. M. Stroud, C. I. Merzbacher and D. R. Rolison, *Langmuir*, 1999, **15**, 674–681.

21. N. Leventis, I. A. Elder, G. J. Long and D. R. Rolison, *Nano Lett.*, 2002, **2**, 63–67.

22. P.A. DeSario, J.J. Pietron, D.H. Taffa, R. Compton, S. Schuenemann, M. Roland, T.H. Brintlinger, R.M. Stroud, M. Wark, J.C. Owrutsky, D.R. Rolison, *J. Phys. Chem. C*, 2015, **119**, 17529–17538.

23. N.Q. Le, I.V. Schweigert, *J. Phys. Chem. C*, 2017, **121**, 14254–14260.

24.P.A. DeSario, J.J. Pietron, A. Dunkelberger, T.H. Brintlinger, O. Baturina, R.M. Stroud, J.C. Owrutsky, D.R. Rolison, *Langmuir*, 2017, **33**, 9444–9454.

25. D.A. Panayotov, J.R. Morris, P.A. DeSario, J.J. Pietron, T.H. Brintlinger, L.C. Szymczak, D.R. Rolison , *Journal of Physical Chemistry C*, 2013, **117**, 15035–15049.

26. F. H. Kaatz, V. G. Harris, D. R. Rolison, L. Kurihara, and A. S. Edelstein, *Appl. Phys. Lett*., 1996, **67**, 3807–3809.

27. K. P. Rice, E. J. Walker, Jr., M. P. Stoykovich, A. E. Saunders, *J. Phys. Chem. C*, 2011, **115**, 1793–1799.

28. G. H. Chan, J. Zhao, E. M. Hicks, G. C. Schatz, R. P. Van Duyne, *Nano Lett*., 2007, **7**, 1947–1952.

29. A. Marimuthu, J. W. Zhang, and S. Linic, *Science*, 2013, **339**, 1590–1593.

30. D. B. Pedersen, S. Wang, S. H. Liang, *J. Phys. Chem. C*, 2008, **112**, 8819–8826.

31. M. D. Susman, Y. Feldman, A. Vaskevich, I. Rubinstein, *Chem. Mater*. 2012, **24**, 2501–2508.

32. J. A. Jiménez, *J. Alloys Compounds*, 2016, **656**, 685–688.

33. P.A. DeSario, J.J. Pietron, T.H. Brintlinger, J.F. Parker, O. Baturina, R.M. Stroud, D.R. Rolison, *Nanoscale*, 2017, **9**, 11720–11729.

34. P. A. DeSario, C.L. Pitman, D.J. Delia, D.R. Rolison, J.J. Pietron, *Appl. Catal. B,* 2019, **252**, 205–213.